Physica E 41 (2009) 500–505

Contents lists available at ScienceDirect

Physica E

journal homepage: www.elsevier.com/locate/physe

Size control of ZnO nanostructures formed in different temperature zones by varying Ar flow rate with tunable optical properties

Umair Manzoor [a,*], Do Kyung Kim [b]

[a] Department of Physics, COMSATS Institute of Information Technology, Plot #30, Sector H-8/1, Islamabad, Pakistan
[b] Department of Materials Science and Engineering, Korea Advanced Institute of Science and Technology, 373-1 Kusong-dong, Yusong-gu, Daejeon 305-701, Republic of Korea

ARTICLE INFO

Article history:
Received 23 June 2008
Received in revised form
6 September 2008
Accepted 29 September 2008
Available online 10 October 2008

PACS:
78.55.−m

Keywords:
A1. Nanostructures
A2. Growth from vapor
B1. Oxides (ZnO)
B2. Optical materials

ABSTRACT

ZnO nanostructures were synthesized by the vapor transport method. ZnO nanocombs, nanowires and nanorods were formed in a single experiment, in high-, intermediate- and low-temperature zones, respectively. A systematic increase in diameters is observed for all the nanostructures when Ar flow is gradually increased. The diameters of these nanostructures were controlled from few 10's of nanometers to few micrometers. Photoluminescence (PL) properties of as-synthesized nanostructures and effect of heat treatment on optical properties and morphology were investigated.

1. Introduction

Nanoscale materials have simulated great interest owing to their importance in basic scientific research and potential technological applications [1–3]. In geometrical morphologies, a variety of nanostructures have been fabricated, including rods [4], wires [5], combs [6] and tetrapods [7], etc. The study of ZnO nanostructures has attracted many research groups because of their excellent optical, electrical, gas sensing and piezoelectric properties [8,9]. Different synthesis methods have been reported for ZnO nanostructures, but the vapor phase method is probably the most extensively explored approach for the formation of ZnO nanostructures [10]. However, morphology and size control of ZnO nanostructures is still an issue and many groups have focused on this problem. Huang et al. [11] have suggested that diameter of nanowires can be controlled by varying Au layer thickness and longer reaction times. Yao et al. [12] reported that the diameter of ZnO nanowires were temperature dependent and substrates placed in low-temperature zone resulted in small diameters of ZnO nanowires.

Hierarchical assembly of nanoscale building blocks (nanocrystals, nanowires and nanotubes) is a crucial step towards realization of functional nanosystems and represents a significant challenge in the field of nanoscale science [13]. Wang et al. suggested that the formation of the nanotips and nanofinger arrays on the two sides of the comb ribbon is a direct result from the surface polarity of ZnO. The polarity of ZnO (0 0 0 1) surface is the key enabling factor to determine the nanostructures grown on the surface. The self-catalyzed process is likely a mechanism for the growth of oxide nanostructures without the presence of foreign metallic catalysts [14]. Pan et al. [15] reported that by simply increasing the growth time, dimensions of the single crystalline combs can be controlled.

In the present study, we demonstrate that systematic size control of different ZnO nanostructures (rods, wires and combs) is possible by carefully controlling the Ar flow rate. Morphology, dimensional control, structural characterization and discussion on the related growth mechanism are presented. Photoluminescence (PL) studies suggested that tuning of optical properties of ZnO nanocombs are possible by annealing. SEM studies give direct evidence that nanostructures are stable and did not degrade even after annealing at higher temperatures.

2. Experimental procedure

ZnO nanostructures were synthesized by the thermal evaporation method. Equal amounts (by weight) of ZnO powder (99.0%, Hayashi Pure Chemical Industries, Osaka, Japan) and carbon black

* Corresponding author. Tel.: +92 51 9235036; fax: +92 51 4442805.
E-mail address: umanzoor@comsats.edu.pk (U. Manzoor).

1386-9477/$ - see front matter © 2008 Elsevier B.V. All rights reserved.
doi:10.1016/j.physe.2008.09.012

were mixed and transferred to an alumina boat. The boat was placed at the center of the tube furnace (internal diameter 52 mm). Au-coated Si substrates were placed at different positions in the tube furnace. Furnace temperature, holding time and oxygen flow rate in all the experiments were fixed at 900 °C, 15 min and 2 sccm, respectively. System was flushed with high-purity Ar for 1 h before starting the experiment. During the experiment, argon was used as carrier gas and the flow rate was controlled from 10 to 150 sccm. The substrate surface appeared white or light gray, indicating the deposition of ZnO. SEM and TEM were used for morphology and size analysis. At least 80 particles were averaged for the particle size measurement using SEM micrographs.

For post-synthesis annealing, comb-shape dendrites were transferred on a Si substrate and heat treated for 1 h at different temperatures in a quartz tube (25 ∅), placed in the tube furnace. A constant flow of O_2 (99.999% pure) at 1 atmospheric pressure with flow rate of 25 sccm was maintained throughout the annealing process. SEM and PL were measured after every heat treatment. Room-temperature PL was measured using Xe lamp with excited wavelength of 325 nm.

3. Results and discussion

Fig. 1 shows the typical SEM images taken from as-prepared ZnO nanostructures along with their formation temperatures. Three different morphologies namely, nanocombs, nanowires and nanorods were observed. Fig. 1(a–c) shows typical images of ZnO nanorods deposited on Au-coated substrates placed in low-temperature zone (800–750 °C). SEM micrographs suggest that the diameter of nanorods increases with increase in Ar flow rate. Size distribution is wider for nanowires synthesized with high Ar flow rates. Fig. 1(d–f) shows ZnO nanowires grown on Au-coated Si substrates, placed in the intermediate temperature zone (850–890 °C). ZnO nanowires also show similar trend, and their diameter and size distribution increases with increase in Ar flow rate. Aspect ratio for nanorods and nanowires is difficult to measure especially with higher flow rates, as the size distribution becomes very wide.

Fig. 1(g–i) shows typical images of ZnO comb-shape dendrites deposited on Au-coated Si substrates in high-temperature zone (900 °C), placed on top of the boat. General morphology of all the nanostructures consists of one-sided comb-shape structures. Secondary arms of these comb-shape dendrites are parallel to one another. It is interesting to note that with low Ar flow rates (up to 25 sccm) the main stem of the nanocombs is nanowires. When the Ar flow rate is increased to 150 sccm, main stem changes to nanobelt/sheet shape morphology (Fig. 1(i)). It may be because the change in Ar flow changes the super saturation, which ultimately changes the morphology of the nanocombs [16]. All the secondary arms appear on one side of wire/sheet and the other side is without any peculiar structures. The diameters of secondary arms are uniform on a single particle in general, and their length may vary slightly from arm to arm. Close examination of these micrographs also suggests that most of these arms have

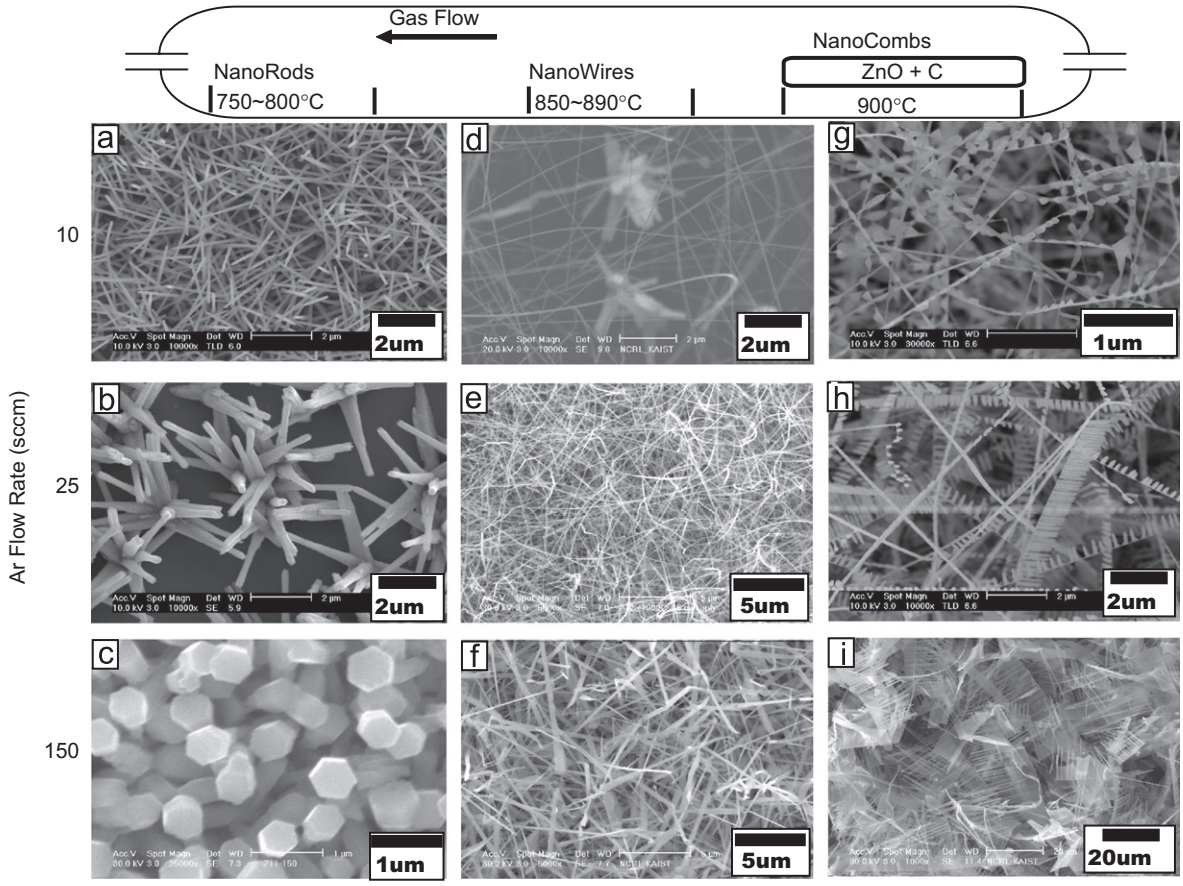

Fig. 1. SEM micrographs of ZnO nanostructures deposited on Si substrates, placed in different temperature zones. Oxygen flow rate was fixed to 2 sccm. Nanorods were deposited in the temperature range of 750–800 °C with Ar flow rate of (a) 10 sccm, (b) 25 sccm, (c) 150 sccm. (d–f) SEM micrographs of nanowires formed in the temperature range of 850–890 °C with Ar gas flow rate of (d) 10 sccm, (e) 25 sccm, (f) 150 sccm, (g–i) SEM micrographs of nanocombs formed at 900 °C with Ar flow rate of (g) 10 sccm, (h) 25 sccm and (i) 150 sccm.

rod-shape morphology with the same diameter all along the length. Also the nanocombs seem to be floating on the substrate, instead of growing with or connected with the substrate. SEM micrographs also suggest that the diameter and secondary arm length of comb-shape dendrites increase with the increase in Ar flow rate. Population density increases and also size distribution is wider for nanocombs synthesized with high Ar flow rates.

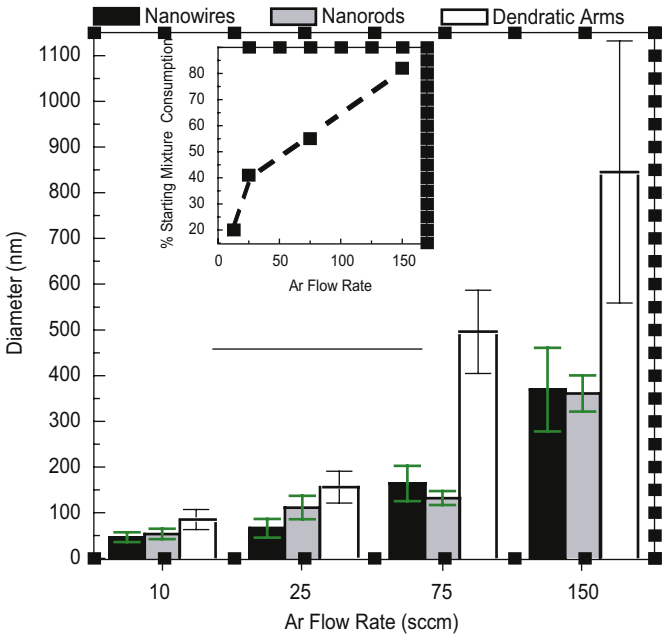

Fig. 2. Bar graph suggests systematic increase in diameter of ZnO nanowires, nanorods and secondary arms of dendritic nanocombs with increase in Ar flow rate. Inset also suggests that consumption of starting mixture also increases with increase in Ar flow rate.

Fig. 2 shows bar graph to demonstrate the effect of Ar flow rate on the diameter of ZnO nanocombs, nanowires and nanorods. The results clearly suggest gradual increase in diameter and wider size distribution with the increase in Ar flow rate for all the nanostructures. In addition, consumption of source material (inset in Fig. 2) increased from 20% to 82% when the flow rate increased from 10 to 150 sccm. Further, higher quantity of the deposited product was obtained i.e., population density was higher with higher flow.

It was first believed that oxygen was present as impurity in the Ar gas and the increase in diameter was because of the increase in the oxygen flow rate [17]. However, experiments performed with only Ar flow of 25 and 150 sccm showed that there was no ZnO deposition and only gold particles were present on Si substrates, suggesting that (i) no oxygen was present in Ar and (ii) oxygen is necessary for the formation of ZnO nanostructures by carbothermal reaction. Therefore, it was assumed that oxygen if present was not responsible for the increase in the diameter of nanostructures. In another set of experiments, the Ar flow was kept constant and oxygen flow was varied. The results (not shown) suggested that the change in oxygen flow rate changes the morphology of the ZnO nanostructures. These results suggested that the change in Ar/O_2 ratio, keeping Ar flow rate constant, changes the morphology. The gas-phase supersaturation determines the growth rate of the structure, and the surface energy of a plane under certain supersaturation decides its activity: growth rate and the proportion in the final structure. Other experimental parameters, such as the temperature of the source material and the substrate, partial

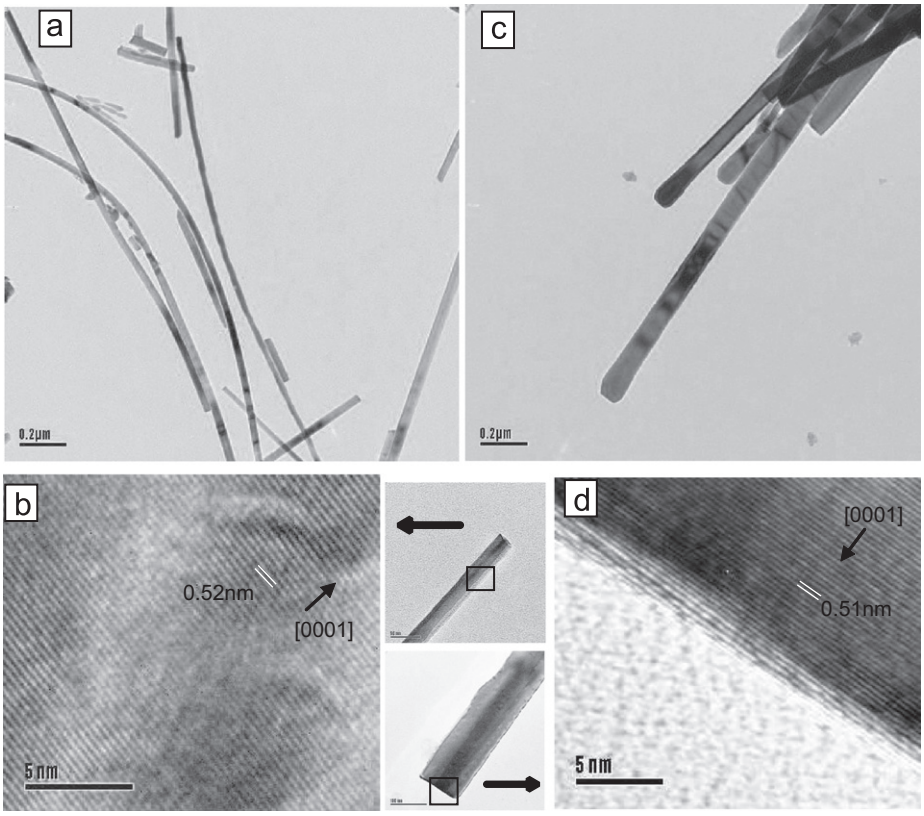

Fig. 3. (a) Low-magnification TEM image of ZnO nanowire synthesized with Ar flow rate of 10 sccm, (b) high-resolution TEM image of single crystalline nanowire showing the lattice fringes suggesting *c*-axis growth and (c) low-magnification TEM image of ZnO nanorods synthesized with Ar flow rate of 10 sccm and (d) high-resolution TEM image of nanorods. The spacing of 0.51 nm between adjacent lattice planes corresponds to (0 0 0 2) crystal planes.

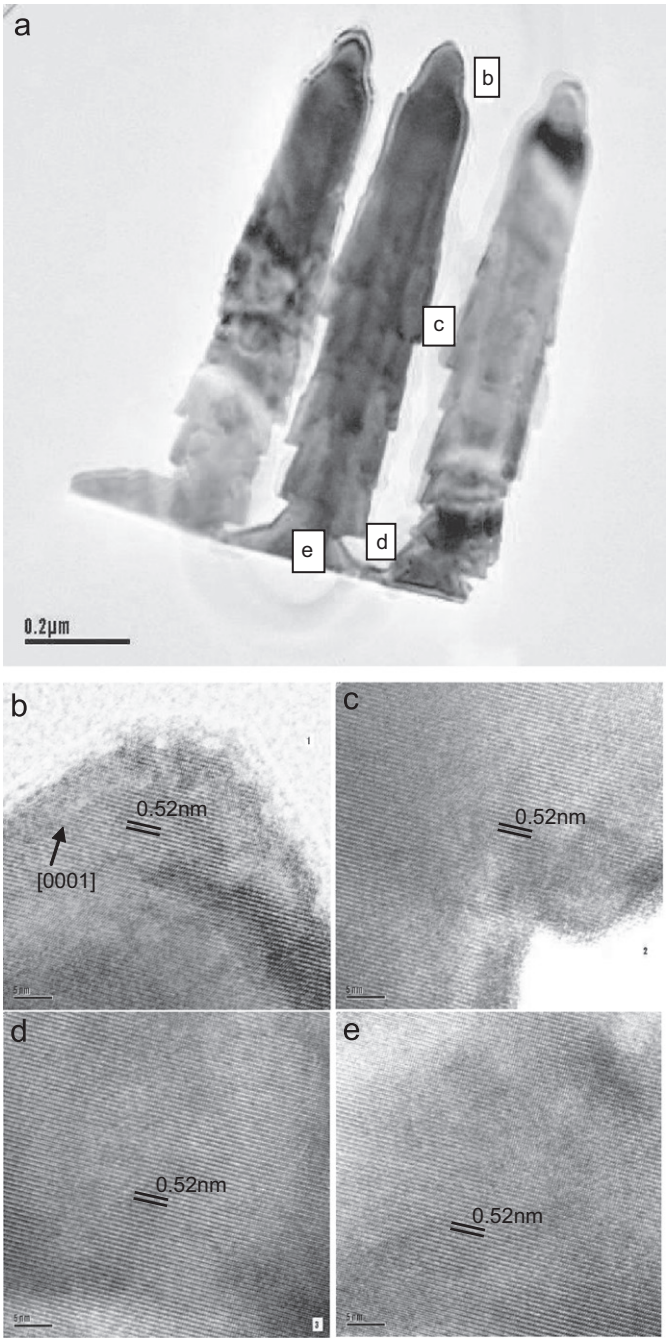

Fig. 4. (a) Low-magnification TEM image of ZnO nanocomb synthesized with Ar flow rate of 25 sccm, (b) high-resolution TEM image of the tip of secondary arm suggesting *c*-axis growth, (c and d) high-resolution TEM image of secondary arm at two different places, (e) high-resolution TEM image of junction of primary and secondary arm. The spacing of 0.52 nm between adjacent lattice planes corresponds to (0 0 0 2) crystal planes.

pressures of Zn species, temperature gradient in the tube furnace, distance from the source material and the substrate, the gas flow rate, the inner diameter of the ceramic tube, and the starting material, all play a role in influencing the final morphology of the structure by entering into the supersaturation term [18,19]. With the increase in the Ar flow rate, higher flux of carbothermal reaction products were generated and also the supersaturation conditions changes, consequently increasing the deposition rate and ultimately size of the nanostructures. Therefore, it can be deduced that size, specially the diameter and the population density of ZnO nanostructures deposited on Si substrates, increases with increase in Ar flow rate. The increase in consumption of the source mixture further strengthened the above statement.

The crystallography of ZnO nanostructures was characterized by transmission electron microscopy (TEM). Fig. 3(a) shows a typical TEM image of ZnO nanowires, synthesized with Ar flow rate of 10 sccm. TEM suggests that most of the wires have smooth surfaces. Further structural characterization of the nanowires was performed in high-resolution mode. Fig. 3(b) shows the high-resolution transmission electron microscopy (HRTEM) image of ZnO nanowires. Lattice spacing of approximately 0.52 nm confirms [0 0 0 1] as the preferred growth direction for ZnO nanowires. TEM micrograph of ZnO nanorods is shown in Fig. 3(c) suggests that nanorods have parallel straight edges and do not show needle-like morphology. HRTEM results are similar to nanorods and Fig. 4(d) confirms single crystalline nature and *c*-axis growth for nanowires.

Fig. 4(a) shows a typical TEM image of ZnO comb-shape dendrites, synthesized with Ar flow rate of 25 sccm. The dendrites are fragile and broken into smaller pieces during TEM sample preparation. The secondary arms of these dendrites have a rough surface and a pointed tip. HRTEM of these nanocombs are shown in Fig. 4(b–e). HRTEM suggests that nanocombs have single crystalline structure and secondary branches have *c*-axis growth direction. XRD analysis (not shown) for all the samples were performed and the XRD results suggested that all the nanostructures were ZnO and no secondary phase of Zn metal was detected. Exact growth mechanism of ZnO nanocombs is still not clear and several speculations such as supersaturation [20,21] and polarization [14] were proposed to account for the formation of these remarkable ZnO combs. More experimental and theoretical work is needed to find the exact growth mechanism.

In addition to study the effect of Ar flow rate on morphology, PL properties of different nanostructures were also investigated. Fig. 5(a) shows PL spectra of ZnO nanostructures formed on different substrates with Ar flow rate of 10 sccm. PL spectrum of all the as-grown ZnO nanostructures mainly consists of an UV emission and defect-related deep-level emission. The PL spectra show shift in visible peak positions for different nanostructures. It is well known that PL spectra in visible zone reflect variation of the stoichiometry in ZnO nanostructures. Vanheusden et al. [22] presented a good correlation between the green emission intensity and the oxygen vacancy density in commercial ZnO suggesting that the green PL in ZnO phosphors is due to the

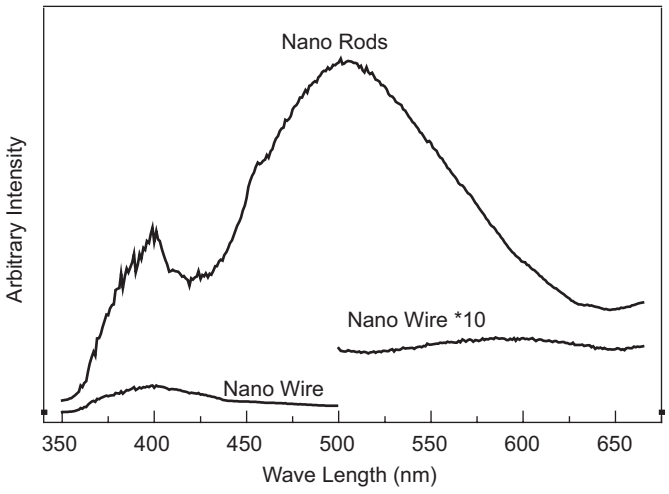

Fig. 5. Room-temperature PL spectrum of the nanostructures was measured using Xe lamp (excited wavelength of 325 nm). PL spectra show significant differences in the visible emission for nanowires and nanorods.

radiative recombination of photogenerated holes with an electron. Peak position in the visible range for nanorods and nanocombs are different than the nanowires. This can be related to the atomic environment of the oxygen vacancy centers. Vanheusden et al. [22] found a correlation between changes in oxygen vacancy centers and the green emission. They have suggested that oxygen vacancy complexes would cause green emission at a slightly longer wavelength than those of the isolated oxygen vacancy centers. The origin of the deep-level green emission of ZnO is not yet understood clearly. But it is generally attributed to structural defects, single-ionized vacancies and impurities [23]. It is suggested that shift in defect-related peaks are because of different types of defects present in nanowires and nanorods owing to different synthesis conditions, i.e. substrate temperature and distance from the source, etc.

ZnO have promising applications in optoelectronic devices, which are sensitive to its crystal perfection. ZnO nanocombs, synthesized with Ar flow rate of 10 sccm, were transferred on a clean Si substrate and post-synthesis annealing in pure O_2 environment was performed to study the effect of annealing on PL properties and morphology. PL spectrum of the as-synthesized ZnO dendrites shown in Fig. 6 mainly consists of strong emission at 398 nm (violet emission) and a prominent defect-related deep-level emissions. After heat treatment in pure O_2 environment, the main peak clearly shows a gradual blue shift (385 nm, after heat treatment at 800 C), which is the well-known direct band emission of pure ZnO [23]. Relative intensity of deep-level emissions also decreases with subsequent heat treatments.

It is generally accepted that deep-level emissions are because of defects, i.e. threading dislocations, oxygen vacancies and zinc interstitials/complexes, etc. [18,24,25]. Jin et al. [26] demonstrated that in pure ZnO, visible violet luminescence is observed from the samples grown in O_2 deficient environment and vanishes when O_2 concentration is increased. It was suggested by a number of researchers that violet emission is because of electron transition from conduction band tail states to valence band tail states, formed due to the mechanical strains and/or structural distortions [27,28]. Increase in annealing temperatures, increases the mobility of atoms and concentration of crystal defects decrease. With the decrease in crystal defects, band tail states and deep-level emissions slowly decreases and a clear blue shift appears in the main peak. However, it is difficult to completely remove the point defects and minor defect-related peaks may always be present [6]. Fig. 6 clearly suggests that intensity of UV peak could be enhanced by annealing and optical properties can be tuned.

Fig. S1 shows the SEM images of a selected nanocomb after every subsequent heat treatment and gives direct evidence that the nanocomb retains its original shape and morphology, after subsequent heat treatments at 600, 700 and 800 °C. In short, it can be concluded that ultraviolet emission of nanocombs can be enhanced significantly, without degradation of nanocombs, by carefully controlling the post-annealing conditions.

Fig. S2 shows XRD results of the same sample before and after subsequent heat treatment. Results suggest that only ZnO peaks are present. After heat treatments at 700 and 800 °C, (1 0 0), (0 0 2) and (1 0 1) peaks shift towards higher angles which are closer to the bulk crystalline ZnO (JCPDS card # 65-3411). Full width at half maximum (FWHM) is also narrower suggesting better crystallinity. Peak shift and narrow FWHM in XRD and higher PL intensity both suggest better crystallinity of ZnO dendrite after heat treatments.

4. Conclusion

In summary, it is demonstrated that the size of ZnO nanostructures can be systematically controlled by carefully controlling the Ar flow rate in the vapor transport process by carbothermal reaction. Morphological control is possible by placing Si substrates in different positions in the tube furnace, which leads to the formation of nanocombs, nanowires and nanorods in high-, intermediate- and low-temperature zones, respectively. Diameters of these nanostructures, show significant increase with increase in the Ar flow. This increase was suggested to be because of higher flux of the carbothermal reaction products with higher Ar flow. Room-temperature PL properties of as-synthesized nanostructures showed prominent defect-related peaks. Post-synthesis annealing suggested that PL emission of ZnO nanocombs can be tuned by carefully controlling the annealing temperatures in oxygen environment. SEM studies give direct evidence that nanocombs are stable and did not degrade even after annealing at 800 °C.

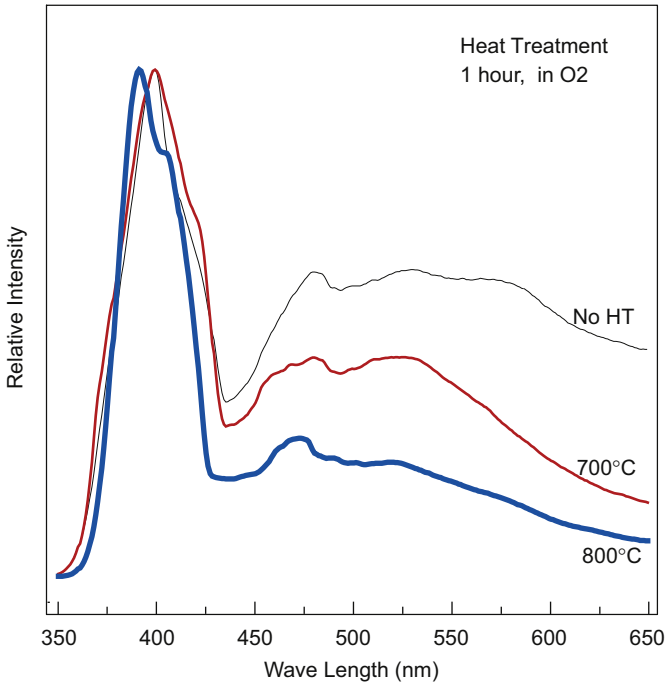

Fig. 6. Room-temperature PL spectrum of the nanocombs after subsequent heat treatment at 700 and 800 °C in oxygen. PL spectra show significant improvement in the UV intensity after every heat treatment.

Appendix A. Supporting information

Supplementary data associated with this article can be found in the online version at doi:10.1016/j.physe.2008.09.012.

References

[1] H.G. Choi, Y.H. Jung, D.K. Kim, J. Am. Ceram. Soc. 88 (2005) 1684.
[2] J. Hu, T.W. Odom, C.M. Lieber, Acc. Chem. Res. 32 (1999) 435.
[3] U. Manzoor, Do Kyung Kim, J. Mater. Sci. Technol. 23 (2007) 655.
[4] Haiping Tang, Zhizhen Ye, Liping Zhu, Haiping He, Binghui Zhao, Yang Zhang, Mingjia Zhi, Zhixiang Yang, Physica E 40 (2008) 507.
[5] H.-Y. Lu, S.-Y. Chu, S.-H. Cheng, J. Cryst. Growth 274 (2005) 506.
[6] U. Manzoor, D.K. Kim, Scr. Mater. 54 (2006) 807.
[7] K. Zhenga, C.X. Xua, G.P. Zhua, X. Lia, J.P. Liua, Y. Yangb, X.W. Sunb, Physica E 40 (2008) 2677.
[8] M. Law, J. Goldberger, P. Yang, Annu. Rev. Mater. Res. 34 (2004) 83.
[9] A. Kolmakov, M. Moskovits, Annu. Rev. Mater. Res. (2004) 151.
[10] Y. Xia, P. Yang, Y. Sun, Y. Wu, B. Mayers, B. Gates, Y. Yin, F. Kim, H. Yan, Adv. Mater. 15 (2003) 353.
[11] M.H. Huang, Y. Wu, H. Feick, N. Tran, E. Weber, P. Yang, Adv. Mater. 13 (2001) 113.

[12] B.D. Yao, Y.F. Chan, N. Wang, Appl. Phys. Lett. 81 (2002) 757.
[13] Y. Wu, H. Yan, M. Huang, B.M. Dr., J.H. Song, P.Y. Dr., Chem.: A: Eur. J. 8 (2002) 1260.
[14] Z.L. Wang, X.Y. Kong, J.M. Zuo, Phys. Rev. Lett. 91 (2003) 185501.
[15] Z.W. Pan, S.M. Mahurin, S. Dai, D.H. Lowndes, Nano Lett. 5 (2005) 723.
[16] Z. Chen, N. Wu, Z. Shan, M. Zhao, S. Li, C.B. Jiang, M.K. Chyu, S.X. Mao, Scr. Mater. 52 (2005) 63.
[17] Y.-K. Tseng, H.-C. Hsu, W.-F. Hsieh, K.-S. Liu, I.-C. Chen, J. Mater. Res. 18 (2003) 2837.
[18] C. Ye, X. Fang, Y. Hao, X. Teng, L. Zhang, J. Phys. Chem. B 109 (2005) 19758.
[19] X. Han, G. Wang, J. Jie, W.C.H. Choy, Y. Luo, T.I. Yuk, J.G. Hou, J. Phys. Chem. B 109 (2005) 2733.
[20] H. Yan, R. He, J. Johnson, M. Law, R.J. Saykally, P. Yang, J. Am. Chem. Soc. 125 (2003) 4728.
[21] J.-H. Park, H.-J. Choi, Y.-J. Choi, S.-H. Sohn, J.-G. Park, J. Mater. Chem. 14 (2004) 35.
[22] K.W. Vanheusden, W.L. Warren, C.H. Seager, D.R. Tallant, J.A. Voigt, B.E. Gnade, J. Appl. Phys. 79 (1996) 7983.
[23] T.Y. Kim, J.Y. Kim, S.H. Lee, H.W. Shim, S.H. Lee, E.K. Suh, K.S. Nahm, Synth. Metals 144 (2004) 61.
[24] H.-J. Ko, M.-S. Han, Y.-S. Park, Y.-S. Yu, B.-I. Kim, S.S. Kim, J.-H. Kim, J. Cryst. Growth 269 (2004) 493.
[25] K. Ogata, K. Sakurai, S. Fujita, S. Fujita, K. Matsushige, J. Cryst. Growth 214/215 (2000) 312.
[26] B.J. Jin, S. Im, S.Y. Lee, Thin Solid Films 366 (2000) 107.
[27] Q.P. Wang, D.H. Zhang, Z.Y. Xue, X.T. Hao, Appl. Surf. Sci. 201 (2002) 123.
[28] S.A. Studenikin, N. Golego, M. Cocivera, J. Appl. Phys. 83 (1998) 2104.